Chemistry and Materials Research
ISSN 2224- 3224 (Print) ISSN 2225- 0956 (Online)
Vol.6 No.5, 2014

Improved pitting corrosion resistance of S.S 316L by Pulsed Current Gas Tungsten Arc Welding

I. Berenjani, A. Bakhtiari, K. Raeissi, M. Shamanian, A. Saatchi
Department of Materials Engineering, Isfahan University of Technology, Isfahan, Iran

Abstract
In this study, S.S 316L was welded using Direct Current Gas Tungsten Arc Welding (DGTAW) and Pulsed Current Gas Tungsten Arc Welding (PGTAW) methods. Optical observations, scanning electron microscopy (SEM) and X-ray diffraction analysis (XRD) were employed to study the effect of continuous and pulse currents on microstructure and phase transformation in weld metal (WM). In addition pits morphology were evaluated by SEM. The corrosion behaviour was analyzed using cyclic polarizaton tests and Mott-schottky measurements. The pulse current resulted in finer grain and more ferrite in WM. This can be due to the decrease in heat input and higher cooling rate encouraged by pulse current. Cyclic potentiodynamic polarization tests showed that the WM of sample produced by pulse current show higher corrosion and pitting resistances than that in sample produced by continuous current. The reason is attributed to lower segregation of solute elements such as chromium and molybdenum into the delta-ferrite and also finer grain size produced in WM due to lower heat input and higher cooling rate. Both of these factors increase the stability of passive layer formed. The results showed that the corrosion behaviour of WM in both conditions (pulse and continuous current) is higher than the base metal (BM). This fact is attributed to the presence of ferrite bands formed in BM due to the segregation of alloy elements. The Mott-schottky plots confirmed that the passive layer formed on welded samples was an n-type semiconductor. The results showed that the samples showed less pitting resistance contained more oxygen vacancies in their passive film structure. It is also concluded that the breakdown of passive layer and pitting formation obey point defect model (PDM).
Keywords: S.S 316L, Pulsed Current Gas Tungsten Arc Welding (PGTAW), lacy ferrite, vermicular ferrite, Pitting corrosion, Mott- Schottky.

1. Introduction

The S.S 316L is a chromium-nickel-molybdenum austenitic stainless steel developed to provide improved corrosion resistance to S.S 304/304L in moderately corrosive environments. The addition of molybdenum improves general corrosion and chloride pitting resistance [1-3]. It also provides higher creep, stress-to-rupture and tensile strength at elevated temperatures. The low carbon content of S.S 316L combined with an addition of nitrogen enables 316L to meet the mechanical properties of S.S 316. The S.S 316L resists atmospheric corrosion, as well as, moderately oxidizing and reducing environments. It also has excellent resistance to intergranular corrosion in the as-welded condition [4].

The S.S 316L is non-magnetic in the annealed condition, but can become slightly magnetic as a result of cold working or welding. It can be easily welded and processed by standard shop fabrication practices. The S.S 316L performs well in sulfur containing service such as that encountered in the pulp and paper industry. The alloy can be used in high concentrations at temperatures up to 38°C. The S.S 316L also has good resistance to pitting in phosphoric and acetic acid. It performs well in boiling 20% phosphoric acid [5]. The higher molybdenum content of S.S 316L assures it will have superior pitting resistance in applications involving chloride solutions, particularly in an oxidizing environment. However, in environments that are sufficiently corrosive to cause intergranular corrosion of welds and heat-affected zones alloy 316L should be used because of its low carbon content [6-8].

The Gas Tungsten Arc Welding (GTAW) is one of the most important joining technologies in welding-related fabrication. High-quality weld joints without spattering and slag qualify this welding technology for the major part of metals. The GTAW is most commonly divided into two methods Direct Current Gas Tungsten Arc Welding (DGTAW) and Pulsed Current Gas Tungsten Arc Welding (PGTAW). In the (PGTAW) mode, the welding current rapidly alternates between two levels. The higher current state is known as the pulse current, while the lower current level is called the background current. During the period of pulse current, the weld area is heated and fusion occurs. Upon dropping to the background current, the weld area is allowed to cool and solidify. Pulsed-current has a number of advantages, including lower heat input and consequently a reduction in distortion and deformation in thin workpieces. In addition, it allows for greater control of the weld pool, and can increase weld penetration, welding speed, and quality. A similar method, 'manual programmed' allows the operator to program a specific rate and magnitude of current variations, making it useful for specialized applications. [9-10].

The pitting corrosion resistance of stainless steels is significantly affected by metallurgical parameters like, cold working, alloy composition, inclusions, heat treatment, grain size, sensitisation, and secondary precipitates

[11].Welding is the main joining method for stainless steels. Welding parameters have strong effect on metallurgical properties by influence on grain size, hardness, residual stress and surface roughness [12].
This paper is focusing on the effects that Pulsed Current Gas Tungsten Arc Welding may have on the corrosion properties of stainless steel 316L, the corrosion behavior was analysis in 3.5% (wt) NaCl solution by cyclic polarization test and Mott-Schottky measurements. Different electrochemical theories were discussed.

2. Experimental procedure

The material used in this study was stainless steel 316L, the chemical composition of the alloy is presented in table 1. The specimens have prepared in 20mm × 40mm × 3mm dimension. The type of filler used was a commercial 316L wire. The chemical composition of the wire is presented in table 2.
Removal of the weld bead was done by milling (Drilling and milling machine, Model ZX7032). The fusion zone and line removed completely before corrosion tests. . Studied were carried out four times and the average of the results considered as the final report.

Table 1 Chemical composition of stainless steel 316L (wt.%).

C	Si	Mn	P	S	Cr	Ni	Mo
0.08	1.00	2.00	0.045	0.030	0.058	10.00-14.00	2.00-3.00

Table 2. The chemical composition of 316L filler metal.

C	Si	Mn	Ni	Cr	Mo
0.02	0.39	1.85	12.20	18.70	2.30

The welding process has done by Direct Current Gas Tungsten Arc Welding (DGTAW) and Pulsed Current Gas Tungsten Arc Welding (PGTAW) methods. The welding parameters are present in table 3 and table 4. In this study specimens welded by (DGTAW) and (PGTAW) marked CW and PW respectively.

Table 3. The process parameters of (DGTAW) method.

Voltage (V)	Current (A)	Velocity (mm/min)	Gas pressure (lit/min)	Input heat (KJ/mm)
16	105	123	6	0.82.

Table 4. The process parameters of (PGTAW) method.

current	Base current	Average current	Voltage*	Current timing (%)	Pressure of argon gas (lit/min)	Frequency ()	Velocity (mm/min)	Input heat (KJ/mm)
155	54	110	16	%55	9	2	153	0.690

* The

The specimens were polished using carbide papers from 80 to 1200 grit. Finally, specimens washed with ethanol and pure water, and then were polishing with 0.3 µm of Al2O3 powder. The electrochemical etch has done in 0.6 HNO3 in 1.1 V potential for 2 minutes.
The scanning electron microscopy (SEM) was employed to study the effect of welding methods on microstructure of stainless steel 316L. In addition, the microstructure of specimens after corrosion tests was studied using SEM. The grain size of (WM) determined using Clemex software. The average number of grain size reported according to ASTM E112.
The XRD analysis (Cu k_α radiations, step size 0.03^o, counting time of 1s. A 2-theta scan was performed between 30^o and 100^o and the integrated intensities of several reflections were measured) has employed to validate phase transformation and percentage of ferrite in (WM). Also, the fraction of ferrite phase have determined by rugged feritscope (Fischer, model FMP 30) with smart probe. The smart probe could estimate volume fraction of magnetic and non magnetic phases in steels by electromagnetic induction method. The amount of ferrite phase measured by two ways, ferrite number (FN) and ferrite percentage, (FN) is a standard number which indicate (FN) values according to equation (1):

$$FN = (vol\%.Fe) \times (-2 \times 0.025813 \times Fe + 5.408679 \times Fe - 102.3902)/100 \qquad (1)$$

In order to perform electrochemical potentiodynamic polarization experiments, cyclic polarization technique and Mott-Schottky measurements were conducted in 3.5% NaCl solution at room temperature. A standard corrosion cell kit consisted of two graphite counter electrodes as the working electrodes and s saturated calomel electrode (SCE) as the reference electrode. The cyclic polarization tests have done after 2 hours immersion time. Potentiodynamic scanning was performed by stepping the potential at a scan rate of 1 mVs^{-1} from 25 mV under open current potential (OCP). In order to study the semiconductors properties of passive film Mott-Schottky measurements has applied. The Mott-Schottky method involves measuring the apparent capacitance as a function of potential under depletion condition and is based on the Mott-Schottky relationship Eq (2):

$$\frac{1}{C_{SC}^2} = \frac{1}{e\varepsilon\varepsilon_o N}(E - E_{FB}\frac{KT}{e}) \quad (2)$$

Where: C_{sc}= capacitance of the space charge region, ε= dielectric constant of the semiconductor, ε_o= permittivity of free space, N= donor density (electron donor concentration for an *n*-type semiconductor or hole acceptor concentration for a *p*-type semiconductor), E= applied potential and E_{FB}= flatband potential.

The Mott-Schottky plots (1/C2 vs. E) are presented *p*-type silicon semiconductor and an *n*-type silicon semiconductor according to slope of plots, *p*-type shows negative slope whereas *n*-type shows positive sloop. The donor density can be calculated from the slope, and the flatband potential can be determined by extrapolation to C = 0. The capacitance values are calculated from impedance measurements.

3. Results and discussion

3.1. Microstructure studies

Fig. 1 shows the typical microstructures of the base metal, CW and the PW specimens, the CW and PW which consist of primary ferrite at the center of solidification cells engulfed by austenite. It was seen in fig 1 (a), one type of ferrite morphology is observed; is known as vermicular. Whereas the PW specimen has two types of ferrite morphologies vermicular ferrite and lacy ferrite and its structural characteristics have significant influence on its properties. The difference in the morphology of ferrite affects low-temperature toughness and corrosion resistance of austenitic stainless steels weld metals. The lacy ferrite finer than vermicular ferrite, the finer microstructure enhanced mechanical and corrosion properties [13].

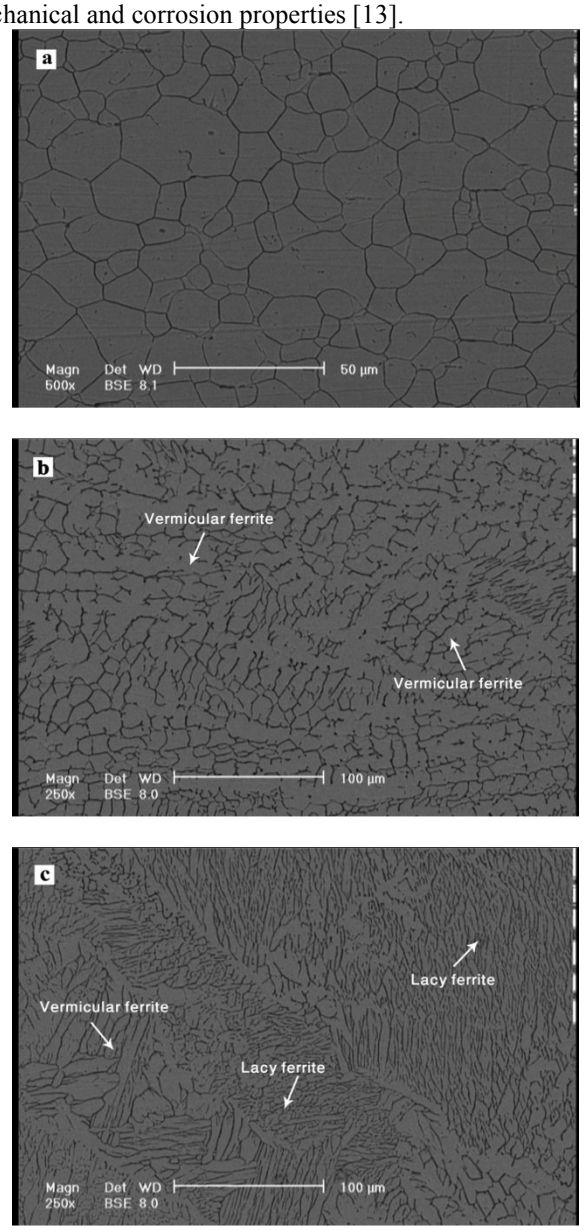

Fig 1. SEM micrograph of the (WM) (base metal (a), CW (b), PW (c))

Most austenitic stainless steel weld and cast metals are designed to solidify to give primary ferrite and secondary austenite to minimize the occurrence of hot cracks. This solidification mode is known as the ferritic-austenitic solidification mode (FA mode) [15-17].
The pulse currents in (PGTAW) method seem to have an indirect influence on the δ-ferrite contents in weld metal. The higher the pulse currents are the higher δ -ferrite content of the weld metal. Welding pulse current may affect on the nitrogen content in the weld metal. The nitrogen content in the weld metal made a finer microstructure [12-18].
Formation mechanisms for vermicular ferrite could be explained as following, at the fusion boundaries, planar austenite first grows epitaxially from the base metal austenite, and then the ferrite nucleates and starts to crystallize on the growing planar austenite. At the nucleation of the ferrite, the parallel relationship between close-packed planes is established between the ferrite and the planar austenite. When the ferrite nucleates with the parallel relationship between close-packed planes, the coherency between the ferrite and the austenite is not so good. The austenite at dendrite boundaries is likely to grow into ferrite at dendrite cores on ferrite-austenite transformation, with planar austenite/ferrite interface, since the planar growth of austenite is a reasonable consequence that minimizes the interfacial energy and avoids the formation of any additional ferrite/austenite interface. Therefore the morphology of the retained ferrite becomes vermicular [19-22].
The lacy ferrite formation was described below; at the fusion boundaries, when the ferrite nucleates on the epitaxially growing planar austenite from the base metal austenite .The ferrite and the planar austenite, plate-like austenite readily grows from the interdendritic region into the ferrite of dendrite core epitaxially along the habit plane[23-25] on ferrite-austenite transformation because of the good coherency between the ferrite and the austenite, and therefore the morphology of the retained ferrite becomes lacy. It is presumed that the growth of plate-like austenite into the ferrite with keeping the coherent ferrite/austenite interface is more favorable than the planar growth of austenite into the ferrite with keeping the incoherent ferrite/austenite interface because the increase in the total interfacial energy of a whole system can be suppressed, regardless of the increase in the ferrite/austenite interface.
Incidentally, it is not easy to specify the factors that decide the parallel relationship between close-packed planes is established between the ferrite and the planar austenite at the fusion boundaries. Nevertheless, it is presumed that the relationship between the preferential growth direction of the austenite and the heat flow direction is one of the possible factors. When the preferential growth direction of the austenite is not aligned with the heat flow direction, the solidification of the planar austenite is delayed [26]. . In such a case, only the small delay of solidification causes a large fall in the liquid temperature at the solidification front where the ferrite nucleates, because the temperature gradient near the fusion boundary is large. As a result, the ferrite that requires a large critical under-cooling for nucleation can easily nucleate, and for this reason, the nucleation frequency of the ferrite with the parallel relationship between close-packed planes is expected to become large. Thus the morphology of the retained ferrite becomes lacy [27-33].
The XRD patterns showed in Fig 2. The XRD results approved presence of ferrite in base metal, CW and PW specimens. The XRD results are given in table 5, according to this table percentage of ferrite of PW specimen more than CW and base metal specimens. In order to increase accuracy of XRD results, amount of ferrite measured by ferritscope. The values of amount of amount of ferrite that calculated by ferritscope are presented in table 6; it is clear the results in a good agreement.

Table 5. The percentage of ferrite calculated by XRD

Specimen	$I_{\gamma\,(111)}$	$I_{\gamma\,(200)}$	$I_{\gamma\,(220)}$	$I_{\delta\,(110)}$	$I_{\delta\,(110)}$	Percentage of ferrite
Base metal	1197	2665	2026	150	40	3.2
CW	1427	646	1866	360	32	6
PW	1188	617	1866	769	55	14.2

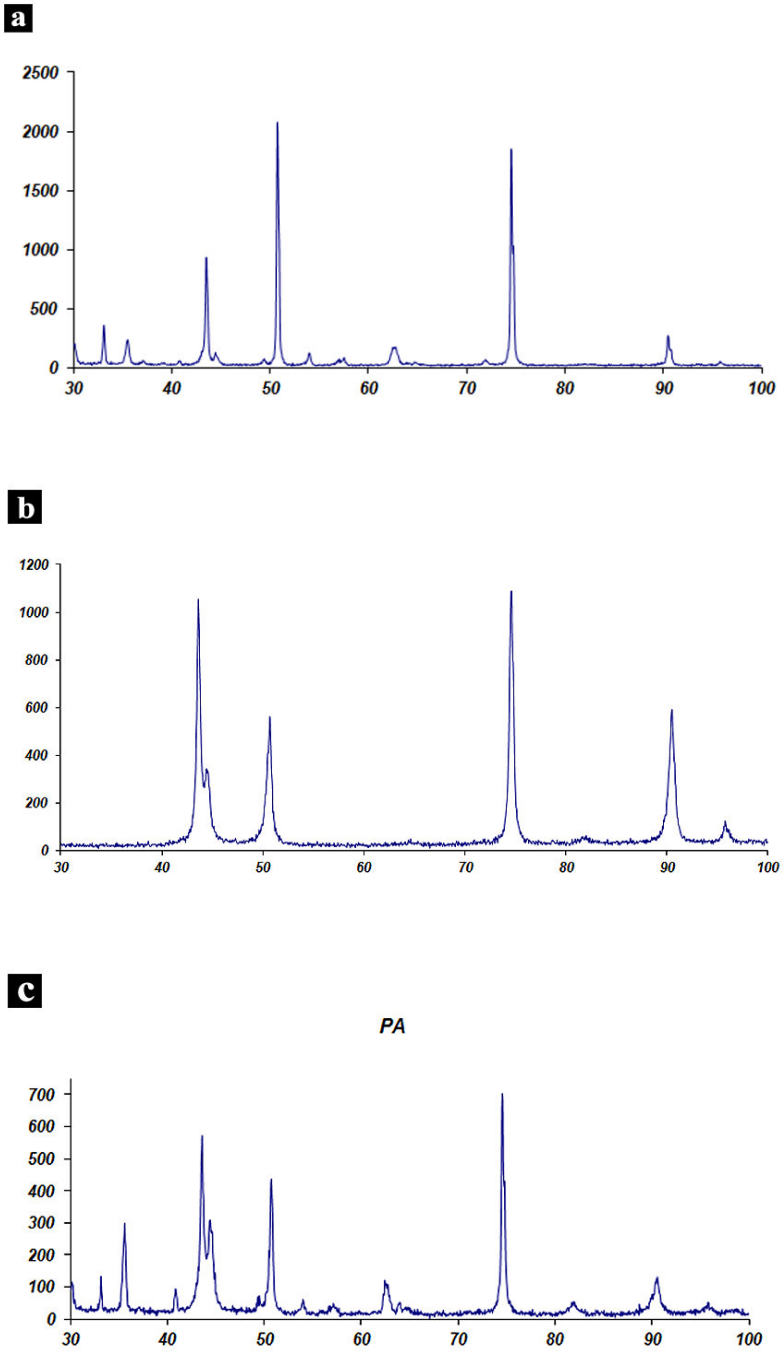

Fig 2. XRD diagrams of the (WM) (base metal (a), CW (b), PW (c))

Table 6. The percentage of ferrite calculated by ferritscope

Base metal	CW	PW
4	7	14

The grain size of specimen was measured by Clemex software, the results of grain size measurements are given

in table 7. It is clear the grain size in PW specimen finer than CW specimen. From the literature survey, it is observed that the process parameters like gun voltage, base current, and welding speed affect the weld quality [33-39].

Table 7. The grain size calculated by Clemex software

Base metal	CW	PW
14	35	18.5

This is due to low heat input and high cooling rate of (PGTAW); grain size gets reduced with the reduction in temperature [40]. The dendrite spacing of weld metal in the constant current is wider but the pulsed current process reveals narrower spacing. The evolution of microstructure in weld fusion zone is also influenced in many ways by current pulsing. Principally, the cyclic variations of energy input into the weld pool cause thermal fluctuations, one consequence of which is the periodic interruption in the solidification process. As the pulsed peak current decays the solid-liquid interface advance towards the arc, it increasingly becomes vulnerable to any disturbances in the arc form. The grain refinement can be rationalized in terms of lower heat input and pulse current effects. The latter also breaks the arms of dendrites, leading to changes of the solidification mode. Thus, the mechanical and corrosion properties improved due to grain refinement. It is assumed the thermal fluctuations made a stormy weld pool and the heat concentrations change its place in weld pool. The changing of thermal behaviour could cause of breakdown of dendretic branches. The particles of broken dendrites are places of hetrogyine nucleation. The hetroyine nucleation encouraged forming finer microstructure. [40-44].
As current augments again in the subsequent pulse, growth is stopped and re-melting of the growing dendrites can also occur. Current pulsing also results in periodic variations in the arc forces and hence an additional fluid flows, which lowers temperatures in front of the solidifying interface. Furthermore, the temperature fluctuations inherent in pulsed welding lead to a continual change in the weld pool size and shape favoring the growth of new grains. It is also to be noted that effective heat input for unit volume of the weld pool would be considerably less in pulsed current welds for the average weld pool temperatures are expected to be low. Thus grain refinement observed in the (PGTAW) welds is therefore believed to be due to effects of pulsing on the weld pool shape, thermal fluctuations, fluid flow and temperatures. The continual change in the weld pool shape is particularly important. As the direction of maximum thermal gradient at the solid-liquid interface changes continuously, newer grains successively become favorably oriented. Thus, the individual grains grow faster in small distance allowing for more grains grow, resulting in a fine grained structure [45]. The other declaration of grain refining is that convection through the melting pool may be the reason of dendrite fragmentation. Dendrite's arms may be separated from the main branch during the use of pulsed current. They can act as inoculants in fusion zone of weld. These two theories are the main reasons of grain refining in fusion zone of (PGTAW).

3.2. Corrosion analysis

The polarization curves in Fig. 3 reveal a self-passivation behavior in all the specimens. The corrosion behaviour consisted of breakdown of passive film and repassivation. The corrosion potential of stainless steel 316L is about -200 mV and the passivation region starts from 375 to 436 mV. The repassivation potentials start from -60 to -30 mV. The results from cyclic polarization tests are presented in table 8.

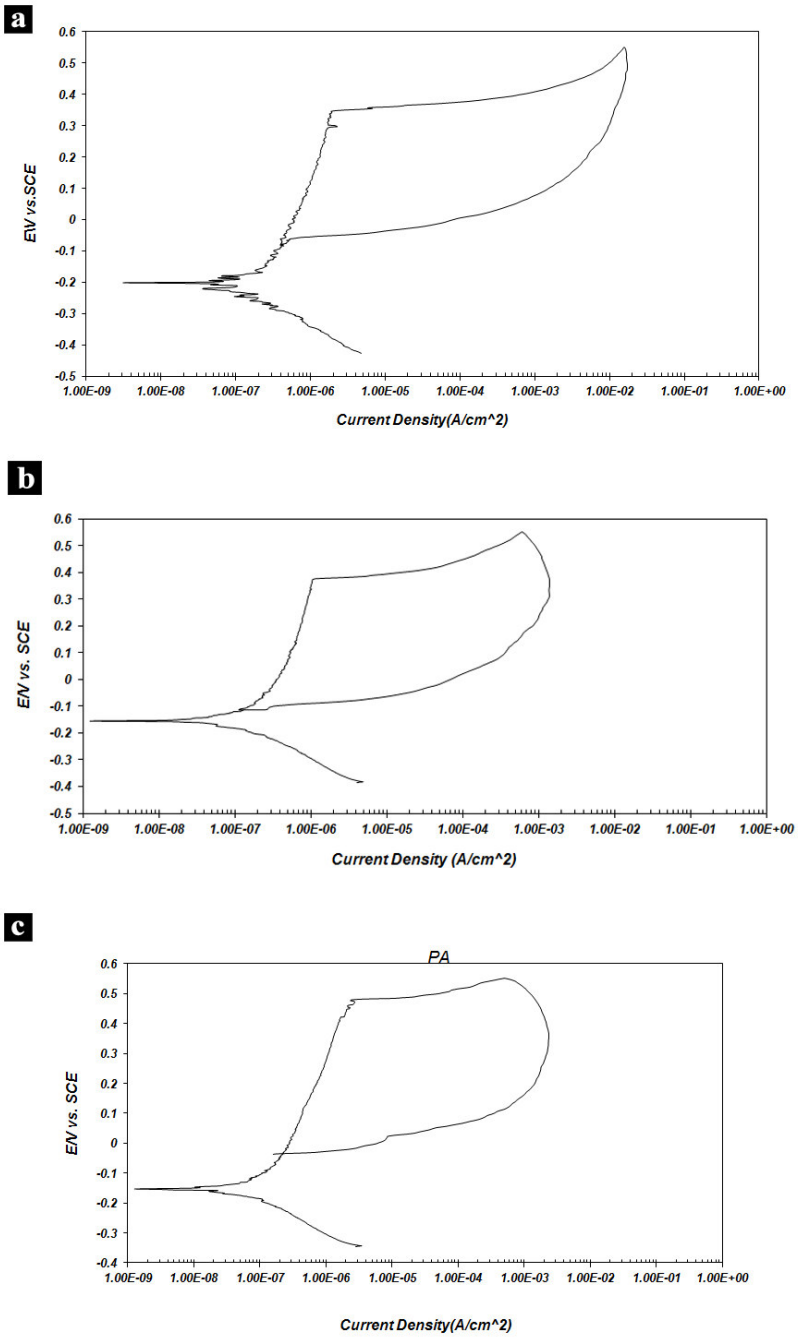

Fig 3. Polarization curves of the (WM) (base metal (a), CW (b), PW (c))

Table 8. The values of I_{Corr} and E_{Corr}

Specimen	I_{Corr} (nA/cm^2)	E_{Corr} (mV)
Base metal	130	-200
CW	230	-254
PW	170	-125

According to cyclic polarization diagrams and table 8, corrosion rate decreased in PW specimen than CW and base metal specimens. The values of corrosion current densities and corrosion potentials (E_{Corr}) indicated better corrosion resistance in specimen that welded by (PGTAW). Because of low heat input and high cooling rate in (PGTAW), rapid solidification has occurred. The rapid solidification doesn't allow alloying elements diffuse and alloying elements distributed uniformly in weld metal. Therefore, the chemical compositions of austenite and ferrite were same and presence of δ-ferrite is benign for weld metal [46]. Moreover, in general the ultrafine grained showed the most positive pitting potential as compared to coarse grained samples. One order of

magnitude decrease in corrosion rate was observed between coarsest and ultrafine grained microstructure. Due to the smaller grain size in (PGTAW) specimen, there are more numerous grains; therefore, more grain boundaries exist. Due to lower free energy of twin boundaries as compared to grain boundaries, the rate of carbide precipitation and corrosion rate is low at these boundaries [47]. It is known that the discrete and discontinuous distribution of the grain boundary carbides improves the mechanical properties of the material, specifically the creep resistance, because these particles effectively pin the grain boundaries and decrease grain boundary sliding [48-50].

Table 9, is shown the values of pitting potential (E_{Pit}), which have obtained from cyclic polarization curves. The (E_{Pit}) could be considered as a standard of pitting corrosion resistance [47-52].

Table 9. The values of E_{Pit}

Specimen	E_{Pit} (mV)
Base metal	357
CW	462
PW	436

According to table 9, (E_{Pit}) of PW specimen more than CW and base metal specimens, difference in (E_{Pit}) values could be analysis independently from corrosion environment. The reduction of microsegration in (PGTAW) and refining of ferrite grain size increasing stability of passive film and improve corrosion resistance of stainless steels [53].

The repassivation potentials (E_{RP}) are given in table 10. The (E_{RP}) is a measure of the tendency of an alloy to undergo localized corrosion in a given environment. It has been reported [7,9,10] that (E_{RP}) is the potential below which stable pitting or crevice corrosion does not occur. Also, (E_{RP}) is relatively insensitive to surface finish as well as prior pit depth as long as propagation exceeds a certain minimum value. The predicted repassivation potential is then compared to the corrosion potential (E_{corr}) in the same environment to determine the susceptibility of an alloy to localized corrosion [54].

Table 10. The values of E_{RP} and E_{Pit}-E_{RP}

Specimen	E_{RP} (mV)	E_{Pit}-E_{RP} (mV)
Base metal	-60	405
CW	-144	519
PW	-35	497

Its clear (E_{RP}) values are more than (E_P) values, it means after pitting occurred, the metal capable to repassivation. The hysteresis anodic cycle (E_P- E_{RP}) important as a standard for repassivation ability. In the lowest values of (E_P- E_{RP}) the repassivation ability increased [30]. Because of presence of molybdenum in base metal the (E_P- E_{RP}) more than PW and CW specimen [38]. Furthermore, PW specimen shows (E_P- E_{RP}) value more than CW specimen, increasing grain size decreased corrosion resistance of passive film.

Figure 4 shows Mott-Schottky measurements for passivated of stainless steel. The sloops of three specimens are positives, n-type semiconductor behaviour is observed for both. Reference steel behaviour can be explained from iron contribution principally located in outer part of oxide (n-type oxides). The slope of semiconductor n-type equal to $2/\acute{\varepsilon}\varepsilon_o eN_D$, where $\acute{\varepsilon}$=40 for forming passive film for iron, $\varepsilon_o=8.854\times10^{-12}$ F m^{-1} and e $=1.6\times10^{-19}$ [55]. The number of oxygen vacancy defects (N_D) determined by Power Suite, the densities of N_D are given in table 11.

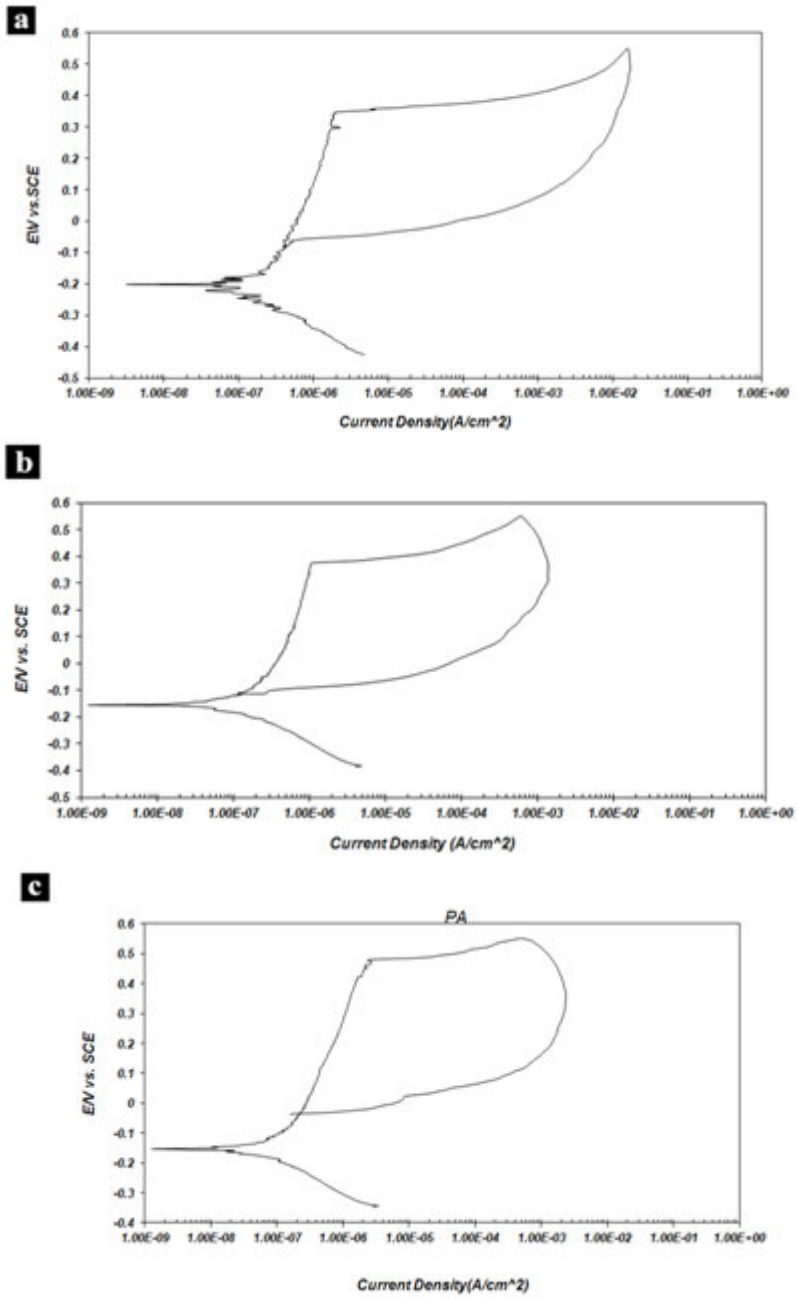

Fig 4. Polarization curves of the (WM) (base metal (a), CW (b), PW (c))

Table 11. The values of $2/\acute{\varepsilon}\varepsilon_o eN_D$ and N_D

Specimen	$2/\acute{\varepsilon}\varepsilon_o eN_D \times 10^{10}$	$N_D\,(m^{-3}) \times 10^{17}$
Base metal	9.78	36
CW	18.26	19
PW	5.38	65

It can be seen from table 11; PW specimen shows the lowest N_D density. Based on PDM model each N_D could absorb Cl^- ion, so passive film produce a N_D for its compensation. New N_D continued absorption of Cl^- ions, this mechanism continued autocatalytic and more cathodic vacancies formed. The concentration of cathion vacancies in the metal/oxide interface increased the probability of breakdown of passive film [54]. Thus increasing the density of N_D in the metal/oxide interface increasing the absorption of Cl^- ions led to passive film breakdown in low potentials [54-55].

SEM investigations in fig 5 have shown the depth and size of pits in the CW and PW specimens. The CW specimen showed greater pit in depth and size than PW specimen. As above mentioned the pitting corrosion

resistance enhanced in (PGTAW) method. In metal with (FA) solidification mode, pitting has occurred in ferrite-austenite interface and developed that austenite corrode selective and ferrite remains [55]. Also, PW specimen shows high capability in repassivation, so repassivation could improve pitting corrosion resistance.

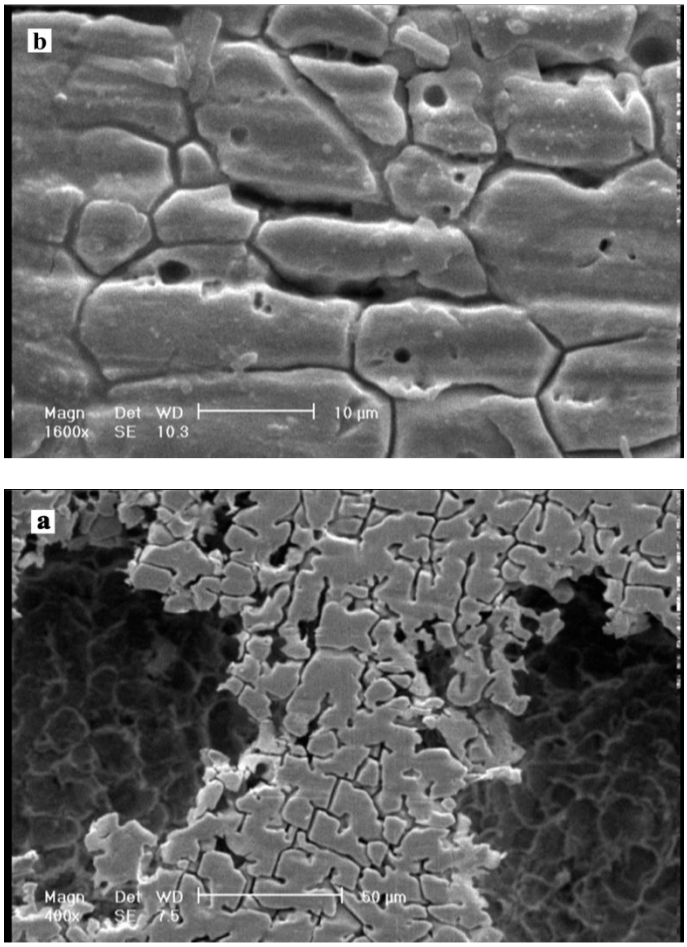

Fig 5. SEM micrograph of the pits (base metal PW (a), CW (b))

4. Conclusion

Based on the results of the metallographic and XRD evaluations of welds and after exposure to 3.5% NaCl solution and evaluation of repassivation film according to Mott-Shotcky measurements can be stated:
The morphology of CW specimen showed one typical form of ferrite, vermicular ferrite. However, PW specimen shows two types of ferrite morphologies, lacy ferrite and vermicular ferrite, the lacy ferrite offer finer structure. The high cooling rate during solidification process and thermal fluctuations produce a finer structure. The XRD results proved presence of ferrite in both CW and PW specimens. The amount of ferrite in PW specimen is higher than CW specimen. The higher amount of ferrite could improve mechanical and corrosion properties. The studies of grin size have indicated PW specimen has finer grain size than CW specimen. The thermal fluctuations propose a tempestuous weld pool that main cause of breakdown of dendritic branches. The particles of dendritic branches encourage heterogenic nucleation. Moreover, the grain refinement can be rationalized in terms of lower heat input and pulse current effects, thus proffer finer microstructure. The electrochemical analyses direct attention to improve corrosion behaviour by using (PGTAW). The pitting resistance in specimen welded by (PGTAW) than other specimens. The PW specimen has shown better repassivation ability than CW specimen; however base metal because of molybdenum and chromium. The Mott-shotcky plots presented n-type behaviour of repassivatin. Furthermore, the PW specimen has lowest N_D density.

Acknowledgements

The authors would like to thank Isfahan refinery laboratories staff and R&D unit engineers for helping with the samples. Assistance received from SEM and XRD laboratories staff of Materials Engineering Department of Isfahan University of Technology (IUT) is also appreciated.

References

[1] Gordon Parr, J., Handson, A., *Introduction to Stainless Steel,* American Society for Metals. 1963.
[2] Sedriks, J.A., *Corrosion of Stainless Steels*, Wiley. 1996.
[3] Molak, R.M., Paradowski, K., Brynk, T., Ciupinski, L., Pakiela, Z., Kurzydlowski, K.J., "Measurement of Mechanical Properties in a 316L Stainless Steel Welded Joint", *International Journal of Pressure Vessels and Piping*, Vol. 86, No. 1, pp. 43-47, 2009.
[4] Hemmingsen, T., Hovdan, H., Sanni, P., Aagotnes, N.O., "The Influence of Electrolyte Reduction Potential on Weld Corrosion", *Electrochimica Acta*, Vol. 47, No. 24, pp. 3949- 955, 2002.
[5] Mudali, U.K., Dayal, R.K., Gill, T.P.S., Gnanamoorthy, J.B., "Pitting Corrosion-Resistance of Nitrogen-Added Type-304 Stainless-Steel Weld Metal with Different Heat Inputs", *Corrosion*, Vol. 46, No. 6, pp. 454-460, 1990.
[6] Senthil Kumar, T., Balasubramanian, V., Sanavullah, M.Y., "Influences of Pulsed Current Tungsten Inert Gas Welding Parameters on the Tensile Properties of AA 6061Aluminium Alloy", *Materials & Design*, Vol. 28, No. 7, pp. 2080-2092, 2007.
[7] Balasubramanian, M., Jayabalan, V., Balasubramanian, V., "Effect of Microstructure on Impact Toughness of Pulsed Current GTA Welded [Alpha]-[Beta] Titanium Alloy", *Materials Letters*, Vol. 62, No. 6-7, pp. 1102-1106, 2008.
[8] Balasubramanian, V., Ravisankar, V., Madhusudhan Reddy, G., "Effect of Pulsed Current Welding on Fatigue Behaviour of High Strength Aluminium Alloy Joints", *Materials & Design*, Vol. 29, No. 2, pp. 492-500 , 2008.
[9] Kumar, A., Sundarrajan, S., "Optimization of Pulsed TIG Welding Process Parameters on Mechanical Properties of Aa 5456 Aluminum Alloy Weldments", *Materials & Design*, Vol. 30, No. 4, pp. 1288-1297, 2009.
[10] Balasubramanian, M., Jayabalan, V., Balasubramanian, V., "Optimizing Pulsed Current Parameters to Minimize Corrosion Rate in Gas Tungsten Arc Welded Titanium Alloy", *International Journal of Advanced Manufacturing Technology*, Vol. 39, No. 5-6, pp. 474-481, 2008.
[11] Uhlig, H.H., *Uhligs Corrosion Handbook,* 2 ed., John Wiley& Sons Inc., New Jeresey,2000.
[12] Lula, R.A. *Stainless Steel*. ASM. 1989.
[13] ASM Metals Handbook, *Properties and Selection Steel Tools Materials and Special Purpose Metals*, 9 ed., ASM, Vol. 3, 1987.
[14] Balasubramanian, V., Ravisankar, V., Reddy, G.M., "Effect of Pulsed Current Welding on Mechanical Properties of High Strength Aluminum Alloy", *International Journal of Advanced Manufacturing Technology*, Vol. 36, No. 3-4, pp. 254-262, 2006.
[15] Tseng, K.H., Chou, C.P., "The Effect of Pulsed GTA Welding on the Residual Stress of a Stainless Steel Weldment", *Journal of Materials Processing Technology*, Vol. 123,No. 3, pp. 346-353, 2002.
[16] Becker, D.W., Adamas, C.M., "Investigation of Pulsed GTA Welding Parameter",*Welding Journal*, Vol., pp. 134-138, 1978.
[17] Reddy, G.M., Gokhale, A.A., "Effect of the Ratio of Peak and Background Current Durations on the Fusion Zone Microstructure of Pulsed Current Gas Tungsten Arc Welded Al-Li Alloy", *Journal of Materials Science Letters*, Vol. 21, No. 20, pp. 1623-1625, 2002.
[18] Babu, S.P.K., Natarajan, S., "Corrosion Behavior of Pulsed Gas Tungsten Arc Weldments in Power Plant Carbon Steel", *Journal of Materials Engineering and Performance*, Vol. 16, pp. 620-625, 2007.
[19] Takalo, T., Suutala, N., Moisio, T., "Austenitic Solidification Mode in Austenitic Stainless Steel Welds", *Metallurgical Transactions*, Vol. Vol.10, pp. 1173-1181, 1979.
[20] Elmer, J.W., Allen, S.M., Eagar, T.W., "Microstructural Development During Solidification of Stainless Steel Alloys", *Metallurgical Transactions*, Vol. 20, pp. 2117-2131, 1989.
[21] Brooks, J.A., Williams, J.C., Thompson, A.W., "Microstructural Origin of the Skeletal Ferrite Morphology of Austenitic Stainless Steel Welds", *Metallurgical Transactions*, Vol.14, pp. 1271-1281, 1983.
[22] Korinko, P.S., Malene, S.H., "Considerations for the Weldability of Types 304l and 316L Stainless Steel", *Welding Journal*, Vol. 1, pp. 61-68, 2001.
[23] Inoue, H., Koseki, T., Ohkita, S., Fuji, M., "Formation Mechanism of Vermicular and Lacy Ferrite in Austenitic Stainless Steel Weld Metals", *Science and Technology of Welding and Joining*, Vol. 5, No. 6, pp. 385-396, 2000.
[24] ASM Metals Handbook, *Corrosion*, 10 ed., ASM, Vol. 13. 1987.
[25] Reclaru, L., Lerf, R., Eschler, P.Y., Meyer, J.M., "Corrosion Behavior of a Welded Stainless-Steel Orthopedic Implant", *Biomaterials*, Vol. 22, No. 3, pp. 269-279, 2001.
[26] Zumelzu, E., Sepulveda, J., Ibarra, M., "Influence of Microstructure on the Mechanical Behaviour of Welded 316 L SS Joints", *Journal of Materials ProcessingTechnology*, Vol. 94, No. 1, pp. 36-40, 1999.
[27] Dadfar, M., Fathi, M.H., Karimzadeh, F., Dadfar, M.R. and Saatchi, A., "Effect of Tig Welding on Corrosion Behavior of 316L Stainless Steel", *Materials Letters*, Vol. 61 , pp.2343-2346, 2007.

[28] Cui, Y., Lundin, C.D., "Austenite-Preferential Corrosion Attack in 316 Austenitic Stainless Steel Weld Metals", *Materials & Design*, Vol. 28, No. 1, pp. 324-328, 2007.
[29] Lo, I.H., Tsai, W.T., "Effect of Heat Treatment on the Precipitation and Pitting Corrosion Behavior of 347 Ss Weld Overlay", *Materials Science and Engineering A*, Vol.355, No. 1-2, pp. 137-143, 2003.
[30] Ibrahim, M.A.M., Abd El Rehim, S.S., Hamza, M.M., "Corrosion Behavior of Some Austenitic Stainless Steels in Chloride Environments", *Materials Chemistry and Physics*,Vol. 115, No. 1, pp. 80-85, 2009.
[31] Blasco-Tamarit, E., Igual-Munó oz, A., Garcia Antoó n, J., Garcia-Garcia, D., "Effect of Aqueous Libr Solutions on the Corrosion Resistance and Galvanic Corrosion of an Austenitic Stainless Steel in Its Welded and Non-Welded Condition", *Corrosion Science*,Vol. 48, No. 4, pp. 863-886, 2006.
[32] Pujar, M.G., Dayal, R.K., Gill, T.P.S., Malhotra, S.N., "Role of Delta-Ferrite in the Dissolution of Passive Films on the Austenitic Stainless-Steel Weld Metals", *Journal of Materials Science Letters*, Vol. 18, No. 10, pp. 823-826, 1999.
[33] Blasco-Tamarit, E., Igual-Munó oz, A., Garcia Antó on, J., Garcia-Garcia, D., "Corrosion Behaviour and Galvanic Coupling of Titanium and Welded Titanium in Libr Solutions", *Corrosion Science*, Vol. 49, No. 3, pp. 1000-1026, 2007.
[34] Wagner, C., *Journal of Electrochemical Society*, Vol. 98, pp., 1953.
[35] Olsson, C.O.A., Landolt, D., "Passive Films on Stainless Steels - Chemistry, Structure and Growth", *Electrochimica Acta*, Vol. 48, No. 9, pp. 1093-1104, 2003.
[36] Macdonald, D.D., "Passivity - the Key to Our Metals-Based Civilization", *Pure and Applied Chemistry*, Vol. 71, No. 6, pp. 951-978, 1999.
[37] Macdonald, D.D., "The Point-Defect Model for the Passive State", *Journal of the Electrochemical Society*, Vol. 139, No. 12, pp. 3434-3449, 1992.
[38] Sato, N., Electrochemistry at Metal and Semiconductor Electrodes, *Elsevier*, 1998.
[39] Kishore Babu, N., Ganesh Sundara Raman, S., Mythili, R., Saroja, S., "Correlation of Microstructure with Mechanical Properties of Tig Weldments of Ti-6Al-4V Made with and without Current Pulsing", *Materials Characterization*, Vol. 58, No. 7, pp. 581-587, 2007.
[40] *Standard Method for Conducting Cyclic Potentiodynamic Polarisation Measurements for Localised Corrosion Susceptibilityof Iron-, Nickel-, or Cobalt-Based Alloys*, *ASTM Standard G61-94*. 1994.
[41] *Standard Practice for X-Ray Determination of Retained Austenite in Steel with near Random Crystallographic Orientation*, ASTM Standard E975-03, 2003.
[42] Jatczak, C.F., Larson, J.A., Shin, S.W., "Retained Austenite and Its Measurements by X-Ray Diffraction", *SAE, Philadelphia*, pp. 14-43, 1980.
[43] Maki, T., Stainless Steel, Progress in Thermo Mechanical Treatment, *Metals and Alloys*, Mc Grow Hill, pp. 290-295.
[44] Garcia, C., Martin, F., de Tiedra, P., Blanco, Y. and Lopez, M., "Pitting Corrosion of Welded Joints of Austenitic Stainless Steels Studied by Using an Electrochemical Minicell", *Corrosion Science*, Vol. 50, No. 4, pp. 1184-1194, 2008.
[45] Giridharan, P.K., Murugan, N., "Optimization of Pulsed GTA Welding Process Parameters for the Welding of AISI 304L Stainless Steel Sheets", *International Journal of Advanced Manufacturing Technology*, Vol. 40, No. 5-6, pp. 478-489, 2009.
[46] Cui, Y., Lundin, C.D., "Evaluation of Initial Corrosion Location in E316l Austenitic Stainless Steel Weld Metals", *Materials Letters*, Vol. 59 ,No. 12, pp. 1542-1546, 2005.
[47] Silva, C.C., de Miranda, H.C., de Santana, H.B., Farias, J.P., "Microstructure, Hardness and Petroleum Corrosion Evaluation of 316l/Aws E309mol-16 Weld Metal", *Materials Characterization*, Vol. 60, No. 4, pp. 346-352 ,2009.
[48] Lee, D.J., Jung, K.H., Sung, J.H., Kim, Y.H., Lee, K.H., Park, J.U., Shin, Y.T., Lee, H.W., "Pitting Corrosion Behavior on Crack Property in AISI 304L Weld Metals with Varying Cr/Ni Equivalent Ratio", *Materials & Design*, Vol. In Press, 2009.
[49] Mudali, U.K., Dayal, R., Gill, T.P.S. and Gnanamoorthy, J.B., "Effect of Heat Input and Microstructure on Pitting Corrosion in AISI 316L Submerge Arc Welds", *Corrosion*, Vol. 44, No. 8, pp. 511-516, 1988.
[50] Lu, B.T., Chen, Z.K., Luo, J.L., Patchett, B.M. and Xu, Z.H., "Pitting and Stress Corrosion Cracking Behavior in Welded Austenitic Stainless Steel", *Electrochimica Acta*, Vol. 50, No. 6, pp. 1391-1403, 2005.
[51] Di Schino, A., Kenny, J.M., "Effects of the Grain Size on the Corrosion Behavior of Refined AISI 304 Austenitic Stainless Steels", *Journal of Materials Science Letters*, Vol.21, No. 20, pp. 1631-1634, 2002.
[52] Di Schino, A., Barteri, M., Kenny, J.M., "Effects of Grain Size on the Properties of a Low Nickel Austenitic Stainless Steel", *Journal of Materials Science*, Vol. 38, No. 23, pp.4725-4733, 2003.
[53] Pujar, M.G., Dayal, R., Malhotra, S.N., Gill, T.P.S., "Evaluation of Microstructure and Electrochemical Corrosion Behavior of Austenitic 316 Stainless Steel Weld Metals with Varying Chemical Compositions", *Journal of Materials Engineering and Performance*,Vol. 14, No. 3, pp. 327-342, 2005.

[54] Vilaps, M., *Prediction of Microsegretion and Pitting Corrosion Resistance of Austenitic Stainless Steel Welds by Modeling*, Technical Research Centre of Finland, VTT Publications. 1999.
[55] Blasco-Tamarit, E., Igual-Munõ oz, A. and Garcia-Antoó n, J., "Galvanic Corrosion of High Alloyed Austenitic Stainless Steel Welds in Libr Systems", *Corrosion Science*, Vol.49, No. 12 ,pp. 4452-4471, 2007.
[56] Cheng, Y.F. and Luo, J.L., "Electronic Structure and Pitting Susceptibility of Passive Film on Carbon Steel", *Electrochimica Acta*, Vol. 44, No. 17, pp. 2947-2957, 1999

The IISTE is a pioneer in the Open-Access hosting service and academic event management. The aim of the firm is Accelerating Global Knowledge Sharing.

More information about the firm can be found on the homepage:
http://www.iiste.org

CALL FOR JOURNAL PAPERS

There are more than 30 peer-reviewed academic journals hosted under the hosting platform.

Prospective authors of journals can find the submission instruction on the following page: http://www.iiste.org/journals/ All the journals articles are available online to the readers all over the world without financial, legal, or technical barriers other than those inseparable from gaining access to the internet itself. Paper version of the journals is also available upon request of readers and authors.

MORE RESOURCES

Book publication information: http://www.iiste.org/book/

Recent conferences: http://www.iiste.org/conference/

IISTE Knowledge Sharing Partners

EBSCO, Index Copernicus, Ulrich's Periodicals Directory, JournalTOCS, PKP Open Archives Harvester, Bielefeld Academic Search Engine, Elektronische Zeitschriftenbibliothek EZB, Open J-Gate, OCLC WorldCat, Universe Digtial Library , NewJour, Google Scholar